Long-period volcano seismicity: its source and use in eruption forecasting

Bernard A. Chouet

At an active volcano, long-period seismicity (with typical periods in the range 0.2–2 s) reflects pressure fluctuations resulting from unsteady mass transport in the sub-surface plumbing system, and hence provides a glimpse of the internal dynamics of the volcanic edifice. When this activity occurs at shallow depths, it may signal the pressure-induced disruption of the steam-dominated region of the volcano, and can accordingly be a useful indicator of impending eruption.

THE science of volcano seismology aims to understand the dynamics of active magmatic systems, determine the physical properties of such systems, and map the extent and evolution of source regions of magmatic energy, all of which represent critical steps in our understanding of eruptive behaviour and in the assessment of volcanic hazards. A volcano is a characteristic manifestation of the interaction of magmatic activity with the surface of the Earth. The important factors defining a volcanic structure are the duration and rate of magma transport, both of which are episodic in character as a result of the inherent instability of magmatic systems at all timescales[1]. This episodicity is reflected in seismic activity, which originates in a volume of the Earth's crust hosting magma transport paths ranging from well defined loci typified by the feeding conduits and rift zones of single symmetric volcanoes, to bifurcating sets of dykes and sills underlying basaltic cinder fields, basaltic flow fields, and large silicic systems. This seismicity manifests itself in two distinct types of process, namely those originating in the fluid and those originating in the solid.

Processes originating in the fluid result in pressure fluctuations caused by unsteady mass transport and/or thermodynamics of the fluid. By their very nature these processes—and, in particular the frequencies of the pressure fluctuations—provide direct informa-

FIG. 1 Typical signatures of long-period events observed at Redoubt, Pinatubo and Galeras volcanoes. Source depths, h, and epicentral distances, r, in km, are indicated above the seismograms. The traces have been aligned according to the onset of the compressional wave marked by the arrow. The signatures are all characterized by a harmonic coda following a signal onset enriched in higher frequencies. These features are best illustrated in the shallow event at Pinatubo (middle trace), where a high-frequency onset lasting ~ 10 s is seen to merge into a quasi-monochromatic coda lasting ~ 50 s.

tion regarding the state of the fluid. Seismic events originating in fluid processes typically include long-period (LP) events and tremor. Long-period events resemble small tectonic earthquakes in duration but differ in their characteristic frequency range and harmonic signature (Fig. 1). Tremor is characterized by a harmonic signal of sustained amplitude lasting from minutes to days, and sometimes for months or longer. In many instances LP events and tremor are found to have essentially the same temporal and spectral components[2,3], suggesting that a common source process, differing only in duration, underlies the two types of event.

Processes occurring in the solid rock manifest themselves mainly in the form of earthquakes associated with shear failures in the volcanic edifice whereas LP events involve volumetric modes of deformation. The former earthquakes act as gauges that map stress concentrations distributed over a large volume surrounding magma conduits and reservoirs. They are named volcano-tectonic (VT) earthquakes to differentiate them from pure tectonic earthquakes occurring at plate boundaries and elsewhere, although they are indistinguishable from the latter in their broadband spectral characteristics.

Volcano-tectonic seismicity is often the first sign of renewed volcanic activity[4–10], and some eruptions have been immediately preceded by strong short-term increases in VT activity[6,10]. Precursory VT activity may last from days[6,10] to months[4,5,7] or even years[6,8,9]. Hence VT seismicity can be both a good long-term sign of potential unrest as well as a good short-term indicator.

In contrast to VT activity, which is generally more spread out in space and time, LP/tremor activity originates in particular locations within the magma plexus where disturbances in the flow are encountered. This property takes special significance at the locus of interaction between the magma conduit and the groundwater system in stratovolcanic edifices, where the internal disruption of the hydrothermal system and subsequent rapidly developing onset of volcanic eruptive behaviour over periods as short as days to weeks, provide a rich source of pressure perturbations and attendant precursory LP activity. Volcanoes in this state of pressurization are vibrantly 'alive' and pulsating.

Although we are not yet at the point in our understanding of either type of seismicity for either to be an infallible prediction tool, in this author's view LP activity shows particular promise because of its potential for understanding the physical processes that lead to its generation and their practical application to eruption forecasting. Accordingly, I will focus here on LP activity.

The work reviewed below has shown that the basic element of LP activity is the underlying pressurization of magmatic and/or hydrothermal fluids and attendant pressure perturbations, either self-excited or forced, which by their coupling to the solid radiate the characteristic signals of LP events. Crucial to the use of LP events for extracting information about the state of the fluid is our
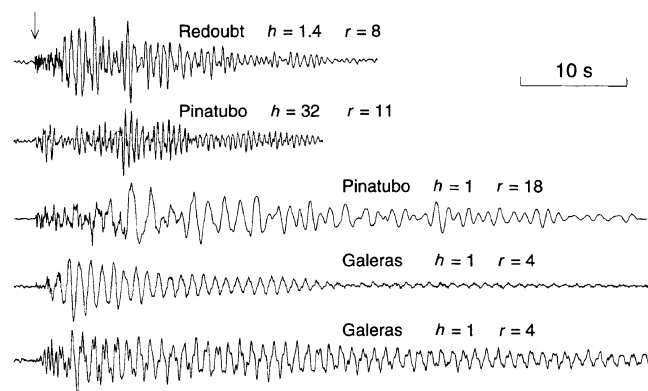
ability to discriminate between LP and VT events. Our studies demonstrate and illustrate that spectral analyses of LP events are needed to recognise the differences between the source properties of fluid-driven activity and those of solid-state failure processes.

Seismic signatures of volcanic activity

The identification of LP events with eruptive activity is scarcely new[11-13], but the significance of this activity for eruption potential was not clearly recognized until a formal theoretical background was established that linked the LP signatures to physical processes at the source. Two outstanding examples of precursory swarms of long-period events are those that preceded the 1958 and 1983 eruptions of Asama volcano, Japan[14-16]. Swarms of long-period events also preceded the 1987 eruption of Meakan-dake, Japan[17], the 1989 Ito-oki submarine volcanic eruption near the Izu peninsula, Japan[18], and the 1982 eruptions of El Chichòn, Mexico[19]. Intense swarms of LP events, some of which were large enough to be recorded at distances of up to 300 km, preceded the paroxysmal eruption of Mount Pinatubo, Philippines, in 1991[5]. Precursory LP swarms were recognized for 14 of 22 significant eruptions at Redoubt, Alaska, in 1989–90[20]. Many additional reports of precursory LP activity can be found in the literature[3,21-31].

Long-period events all share a characteristic signature consisting of a high-frequency onset followed by a harmonic waveform containing one or up to several dominant periods in the typical range of 0.2–2 s (Fig. 1). The high-frequency beginning of the signal is most clear when observations are made close to the source where the effects of anelastic attenuation are minimized (see Fig. 1). An important limitation in recognizing LP seismicity as diagnostic of impending eruptive activity has arisen from the wide variety of names used to describe it. For example, in Japan LP events have been identified variously as b-type events[14,32], N-type earthquakes[15], tremor-like volcanic earthquakes[16], single-frequency earthquakes[17] and isolated tremor[18]; at El Chichòn volcano they were named type-2 and type-3 earthquakes[19], and at Galeras volcano they were referred to as screw-type events[33] and butterfly-type events[34]. Although there is no one-to-one correspondence between these events and those in Fig. 1, there is no mistaking the resemblance between these waveforms. Another impediment has been the idea that the LP signature reflects wave propagation effects along the transmission path[35] rather than characteristics of the source mechanism as accumulating evidence now strongly suggests.

The essential features of the LP signature become clearer when they are compared to those of VT earthquakes or tremor. For example, Fig. 2 shows seismograms and their associated spectrograms for several sources observed before the 14 December, 1989 eruption of Redoubt volcano, Alaska. The LP event is characterized by a weak high-frequency onset with frequencies up to 13 Hz, followed a few seconds later by a strong harmonic signal with a peak frequency near 1.5 Hz lasting roughly 30 s. In contrast, the deeper VT earthquake is dominated by broadband P and S phases with energy peaking in the band of 6–8 Hz, followed by a very short broadband coda (the trailing part of the seismogram) with significant energy up to 15 Hz. This signature is typical for VT sources deeper than a few kilometres and is easily distinguished from that of LP events. The shallow VT earthquake resembles the deep VT event but displays a slightly longer, narrower-band, coda exhibiting frequencies characteristic of a dispersed surface wave-train. Shallow VT earthquakes usually generate stronger surface waves than the deeper VT earthquakes but are still distinguishable from the LP signature. The hybrid event shows mixed characteristics reminiscent of both LP and VT events. The high-frequency onset of the hybrid is more pronounced than that of the LP, but its coda is dominated by a non-dispersive harmonic wavetrain that is characteristic of LP events so that the spectrograms of the codas of hybrid and LP events are similar. In terms of first motions, the VT and hybrid earthquakes both show mixed polarities at the recording stations, whereas LP events typically display the same polarity at all stations[36]. Hybrid events can usually be distinguished from

LP events on the basis of this polarity distribution. The LP, hybrid and shallow VT events in Fig. 2 all occurred in roughly the same source region at depths of 1.4–1.7 km beneath the crater of Redoubt, yet their temporal and spectral signatures are quite distinct. As they were all recorded at the same location, their distinct character cannot be attributed to a path effect. Comparisons with the signatures of a chemical explosion detonated in the crater of Redoubt also indicate that these features can not be attributed to site effects[2]. The tremor signal closely resembles that of the LP event except in its sustained character. The two types of event share the same dominant frequency near 1.5 Hz, and the tremor displays occasional bursts of high frequencies (see signal near 20 s) reminiscent of those found in the early part of the LP signature. These features are suggestive of a common source process, differing only in duration, underlying LP events and tremor.

Source dynamics

The above considerations naturally lead to a classification of seismic events based on the physics of the source process, which has the advantage of offering a clearer picture of the link between fluid transport and seismicity. Viewed in such a context, the enormous variety of seismic signatures observed in volcanoes is merely a reflection of the effects of extreme structural heterogeneity and strong topography of volcanic edifices on the signals originating in two basic families of processes. The first family consists of volumetric sources, in which the fluid plays an active role in the generation of elastic waves, and the second consists of shear or tensile sources involving brittle rock failure.

In volumetric sources, gas, liquid and solid are dynamically coupled and elastic radiation is the result of processes originating in the physics of multi-phase fluid flow through cracks and conduits. Long-period events, tremor and seismic signals related to mechanisms of degassing in open vents are manifestations of such processes. The liquid and gas may be of magmatic or geothermal origin depending on the volcanic setting, and the gas content may vary greatly according to source depth and gas fugacity. For example, the sources of long-period events and tremor beneath Kilauea are thought to involve magma with some gas, the proportion of which increases with the shallowness of the source[3,37,38]. In contrast, the shallow long-period events and tremor under Nevado del Ruiz are interpreted as originating in the thermal interaction between magmatic heat and a separated groundwater system, such that liquid water and steam are the primary constituents of the two-phase fluid involved in the source process[23,24,38]. At Galeras, shallow LP activity appears to be intimately linked to the accumulation of SO_2 beneath the crater floor[31].

The second family of sources involves brittle failure and purely elastic processes. These include the VT earthquakes, in which magmatic processes provide the source of elastic strain energy that leads to rock failure, but where a fluid is not actively involved in the source dynamics—although fluids may be passively involved by reducing effective stress and strength through elevated pore pressures. These sources occur in the brittle rock around the magma reservoir and conduit (either within the volcanic edifice or in the crust beneath it) and may involve shear linked to stresses induced by magma movement[29,39,40], or tensile failure of rock caused by thermal contraction due to cooling in the vicinity of a magma body or in the volcanic edifice as a whole[41,42]. Thus, these sources are associated with the structural response of the volcanic edifice to the intrusion and/or withdrawal of fluids. In this sense they differ from purely tectonic earthquakes, which are driven by large-scale tectonic plate motions, although their source processes and signatures are indistinguishable from those of tectonic events.

In the greater dynamical context of an entire volcanic structure, LP events, tremor and VT earthquakes are intimately related and inseparable. Thus, there must be classes of events that represent the transitions between the idealized end-member families

described above. These correspond to the so-called hybrid events seen in Fig. 2, which are thought to involve shear faulting on a plane intersecting a fluid-filled crack and thus may contain both shear and volumetric components. Consequently, there should be tremor and/or LP-induced failure cascades in which the percolation of fluids through fluid-induced fractures associated with magma transport activates a cascade of shear failures[38,39,43,44]. If true, this means that there should be some sets of hybrid events blending the characteristics of LP events, tremor and VT earthquakes. This is supported by the fact that LP events and tremor in Hawaii volcanoes are clustered within or near clusters of VT earthquakes[43]. This may well be true also for two-phase groundwater systems at high enough pressures to induce shear failures by hydrofracture, as suggested for the hybrid events observed at Redoubt[36].

An interesting aspect of LP seismicity is the similarity in the signatures of individual events in some swarms, which is strongly suggestive of the repetitive excitation of a stationary source in a non-destructive process[2,20,27,32,36]. Another important clue comes from the observed similarities between LP events and tremor. Both have been observed to occur concurrently with the same spatial, temporal and spectral characteristics[2,3]. Both display strongly peaked spectra with dominant frequencies that are independent of azimuth and distance to the source[2,45]. Both show correlations between changes in their spectra and changes in volcanic activity[3,45,46], and both can display wide variations of spectral amplitude and corresponding small variations in frequency during steady activity[3,30].

The repetitive nature of LP seismicity, together with the ringing characteristics of the LP signature and the close link between LP events and tremor, all point to a source effect involving some form of resonant excitation in a fluid-filled conduit. Tremor and LP activity are thus different manifestations of the same basic process of unsteady mass transport. In this context, the LP event may be viewed as the response of the tremor-generating system to a sudden pressure transient, whereas sustained tremor may be interpreted as the response of this system to sustained pressure fluctuations. The occurrence of one or the other depends on the physical parameters of the fluid and flow conditions in effect at the time so that the richness of the signatures observed is a direct consequence of the sensitive dependence of the nonlinear fluid dynamics on these flow parameters. Recent pre-eruptive sequences observed at Redoubt[2,20], Pinatubo[5,47], Galeras[21,25,31] and Ito-oki[48] are examples of this variability of behaviour.

Put together, these observations suggest the working hypothesis that shallow LP activity, and tremor, are manifestations of pressurization in a magmatic/hydrothermal system. Accordingly, one might expect that a direct link should exist between the strength of LP activity and the potential for explosive activity; in other words, one might expect LP events to be more likely to develop into an energetic swarm in explosive systems supporting strong pressurization, than in effusive systems for which pressurization is obviously weaker. By the same token, one might expect that the rate of LP production should depend on the rate and magnitude of pressurization. Thus, a sealed system may support strong pressurization, which may manifest itself in an energetic LP swarm, whereas a leaky system may sustain little pressurization and relatively few LP events. Observations at Redoubt in December 1989 and Galeras in January 1993 provide contrasting cases of pressurization in sealed versus leaky systems. Redoubt, which was capped by a lava dome at the time[2,49], is an example of a sealed system with well developed precursory LP activity. In contrast, Galeras, which had been left with a relatively unobstructed conduit after the July 1992 explosion[31], is an example of leaky system with subtle precursory activity. At Redoubt, the pre-eruption rate of LP production was a few events per minute over a period of about a day[2], and at Galeras the rate was 1 or 2 events per day over a two-week period[21]. Examples of weak LP swarms were those seen during the waning phase of the 1989–90 Redoubt eruption sequence[20]. The most energetic LP activity

encountered to date, both in terms of event magnitudes and rate of event production, was that observed during the week preceding the paroxysmal eruption of Mount Pinatubo on 15 June, 1991[5,50].

It naturally follows that LP activity may also be triggered by depressurization associated with eruptive activity. This has indeed been observed at Redoubt[20] and Galeras[33]. At Kilauea, LP activity and weak tremor have been observed following eruptive episodes at Mauna Ulu in 1969, and are often observed during deflation episodes of the Kilauea summit[3].

Thus, LP events offer a glimpse into fluid dynamics and can be extremely useful in assessing the internal state of a volcano. To use the forecasting potential of shallow LP events fully, however, one must first be able to distinguish their signatures from those of VT earthquakes, a task made difficult by the extreme heterogeneity of volcanic media.

Source modelling

One tool used by volcano seismologists to discriminate between different source types is the comparison of spectral and temporal
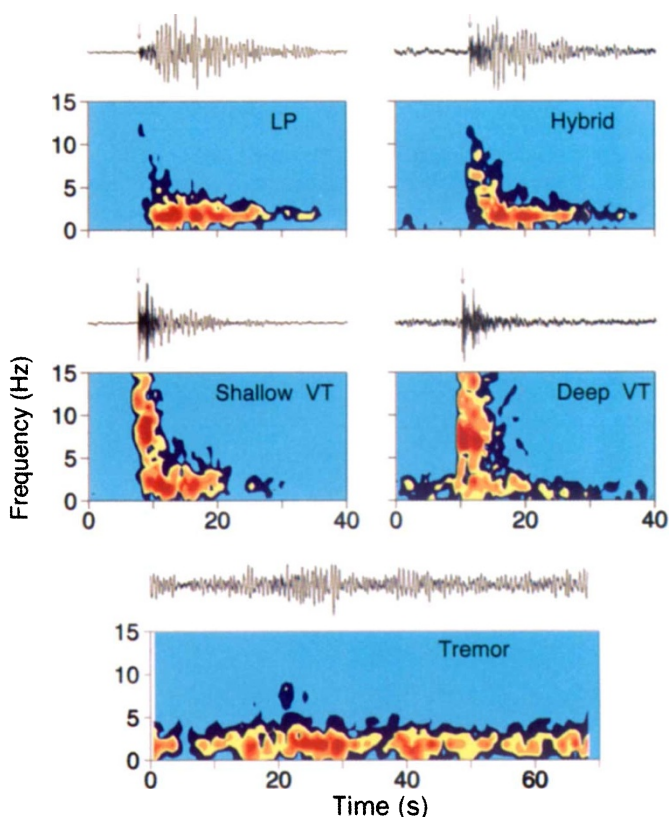

FIG. 2 Vertical ground velocities and associated spectrograms for typical LP, VT and hybrid events and tremor observed at Redoubt volcano. Each spectrogram is a map of the spectral amplitudes of ground velocity versus frequency and time calculated with a moving 1-s window running through the entire seismogram shown above the spectrogram. Warm colours (red, orange and yellow) define the dominant spectral amplitudes; cooler colours (dark and light blue) define lower amplitudes and background. The LP and hybrid events both occurred in a small source zone 1.4 km below the crater floor of Redoubt. The shallow VT earthquake originated 1.7 km below the crater floor, and the deep VT earthquake originated 8.4 km below the crater floor. The tremor displays the same dominant frequency as the LP and hybrid events, but differs from those events in its sustained signal. A small packet of high frequencies 20 s into the tremor seismogram may represent an individual LP event. This tremor is thought to originate from the same source as the LP event. All events were observed at the same receiver location at an epicentral distance of 7.7 km. The origin of the time axis is arbitrary; event onsets are marked by an arrow.

signatures for sources sharing similar locations. Such an approach was taken at Mount St Helens to emphasize the narrow bandwidth of LP events versus the broadband characteristics of VT events[30]. A similar approach was used at Redoubt (Fig. 2), where the LP signatures were also contrasted to the records of a chemical explosion detonated in the crater, which indicated conclusively that the LP signatures were not due to path or site effects[2]. Another powerful tool is the comparison of the power spectra of LP events recorded at widely separated stations. This technique can be used to show that LP spectra share many common peaks among sites for which the wavefields are uncorrelated, a finding which provides a strong argument in favour of a source effect rather than path or site effects. For shallow sources, resonances in near-surface layers often combine with source resonances to make the identification of spectral peaks in the source more difficult. For repetitive sources, stacking the spectra from many individual events may help the identification task by improving the signal-to-noise ratio, but in other cases there may be no alternative other than to have observations at close range where path effects do not completely mask the distinctive characteristics of LP events. Once common spectral peaks have been identified in the wavefield of a LP event, the next step is to test whether the distribution of such peaks is compatible with the overtones of a resonator. A source model that successfully produces the spectral peaks can then be used to infer source parameters such as source geometry, fluid properties and pressure–space–time history.

Although many geometries are possible resonators, including fluid-filled pipes[51], spheres[52] and cracks[38,53,54], I will focus here on the crack model on the grounds of its ability to explain seismic data while at the same time satisfying mass transport conditions at depth in a volcano. The resonance characteristics of a fluid-filled crack depend on the crack geometry, the physical properties of the fluid and solid, the spatio-temporal characteristics of the pressure fluctuations driving the crack, and the boundary conditions in effect at the crack perimeter. For a rectangular crack the geometrical parameters are expressed by the dimensionless ratios L/d and W/L, where L, W and d represent the length, width and aperture of the crack, respectively. Similarly, the properties of the fluid and solid are expressed by the dimensionless ratios α/a, ρ_s/ρ_f and b/μ, where α is the compressional wavespeed and μ is the rigidity of the solid, a is the acoustic wavespeed and b is the bulk modulus of the fluid, and ρ_s and ρ_f are the densities of the solid and fluid, respectively. Two parameters control the crack resonance, namely the crack stiffness C and impedance contrast Z.

The crack stiffness, defined as[38,53-55]

$$C = \frac{b}{\mu}\frac{L}{d}$$

affects the dispersion characteristics of the crack wave sustaining the crack resonance and thereby fixes the resonant frequencies produced by the source. The phase velocity of the crack wave decreases with increasing values of the crack stiffness, so that a crack with large aspect ratio L/d or large contrast b/μ may be capable of producing long-period signals. The impedance contrast between fluid and solid, defined as[38,55]

$$Z = \frac{\rho_s}{\rho_f}\frac{\alpha}{a}$$

affects both the frequency and duration of the radiated signal. The presence of gas bubbles can drastically reduce the sound speed of the fluid[56] so that resonance at a long period may be possible in a short crack. The effect of these bubbles is also to increase the impedance contrast, which increases the duration of the signal. Fluid viscosity contributes another parameter to the description of the source that describes viscous energy loss in addition to radiation loss. Besides its direct effect on signal duration, this viscous dissipation factor does not contribute much to source complexity[38,54] and is not discussed further here.

The spectrum radiated by the crack represents the interference pattern between the longitudinal and lateral modes of resonance, which depends on the ratio W/L and the two parameters C and Z. Beyond these factors, which represent the coupling between the elastodynamics of the solid and acoustics of the fluid via the crack geometry, source complexity is a direct result of the spatio-temporal characteristics of the pressure field associated with the rich nonlinear dynamics of the fluid.

Long-period events recorded at Galeras (Fig. 1) offer graphic examples of the effect of impedance contrast on the duration of the signal. For example, Fig. 3 compares the Galeras data to synthetic seismograms calculated for a vertical fluid-filled crack of rectangular shape embedded in a homogeneous half-space. The synthetics represent the ground response to the crack excitation owing to a sudden step in pressure applied over a small area of the crack wall near the centre of the crack. The good match between data and synthetics suggests that, to first order, the slot-like fluid-filled crack model provides a simple geometry consistent with observations. The fit requires an impedance contrast of 15, which is strongly suggestive of a gas-filled cavity.

The situation at Galeras may have been close to optimum in terms of the relative importance of source versus path effects. The source depth of $1(\pm0.2)$ km and epicentral distance of $1(\pm0.1)$ km were such that multiple reflections in thin soft surficial layers draping the volcano were apparently minimized. At the same time the sustained resonance of the source associated with the strong impedance contrast sharpened the definition of the spectral peaks (Fig. 3c) making their identification easier. The situation is considerably more complex when the source is embedded in soft shallow layers and the impedance contrast is weak.

To illustrate the effect of medium heterogeneity on the radiation from a low-impedance fluid-driven crack, I now consider the case of a Hawaiian basaltic magma. Figure 4a compares synthetic seismograms of the vertical component of ground velocity calculated for a vertical crack embedded in a layered structure with those calculated for the same source embedded in a homogeneous half-space. The fluid in the crack has a sound speed of 1.25 km s^{-1}, which is compatible with a basaltic magma containing a void fraction of gas of about 0.05%, and the impedance contrast is near 1. The layered structure is appropriate for the area of Pu'u O'o crater on the east rift of Kilauea[57] (see Fig. 4 legend), and the homogeneous half-space has parameters identical to those found in layer 3 of that structure.

The low impedance contrast accounts for the poorly developed source resonance, as demonstrated by the weak harmonic coda in the synthetics calculated for the homogeneous medium. Whereas

FIG. 3 Comparison between data and synthetics for an LP event that preceded the 14 January 1993 eruption of Galeras volcano. a, Vertical ground velocity recorded at a distance of 1 km from the crater. b, Vertical ground velocity calculated at the same location for the excitation of a vertical fluid-filled crack buried at a depth of 1 km beneath the vent of Galeras. c, Spectrum for data (thin line) and synthetics (dotted line). The source model has the following parameters: crack length, 180 m; crack width, 90 m; crack aperture, 0.05 m; crack stiffness, 100; sound speed of fluid, 0.3 km s^{-1}; compressional wavespeed of solid, 2.5 km s^{-1}; density ratio of fluid to rock, $\sim$ 0.5; and ratio of bulk modulus of fluid to rigidity of rock, 0.025.
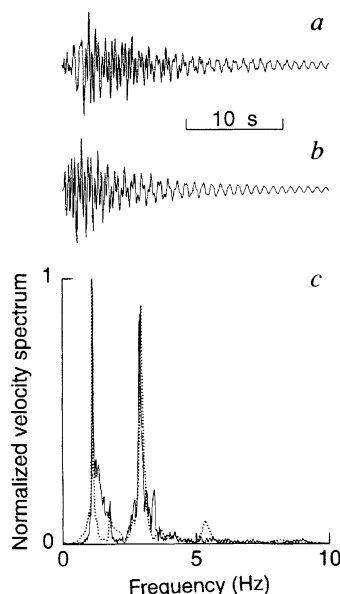
these synthetics are dominated by sharp P, S and Rayleigh phases, those derived for the layered medium present a distinctive spindle-shaped signal, in which crack oscillations appear as a short-duration quasi-monochromatic coda emerging out of the broader-band contributions from near-surface layer resonances. At first glance, this would seem to make the task of distinguishing
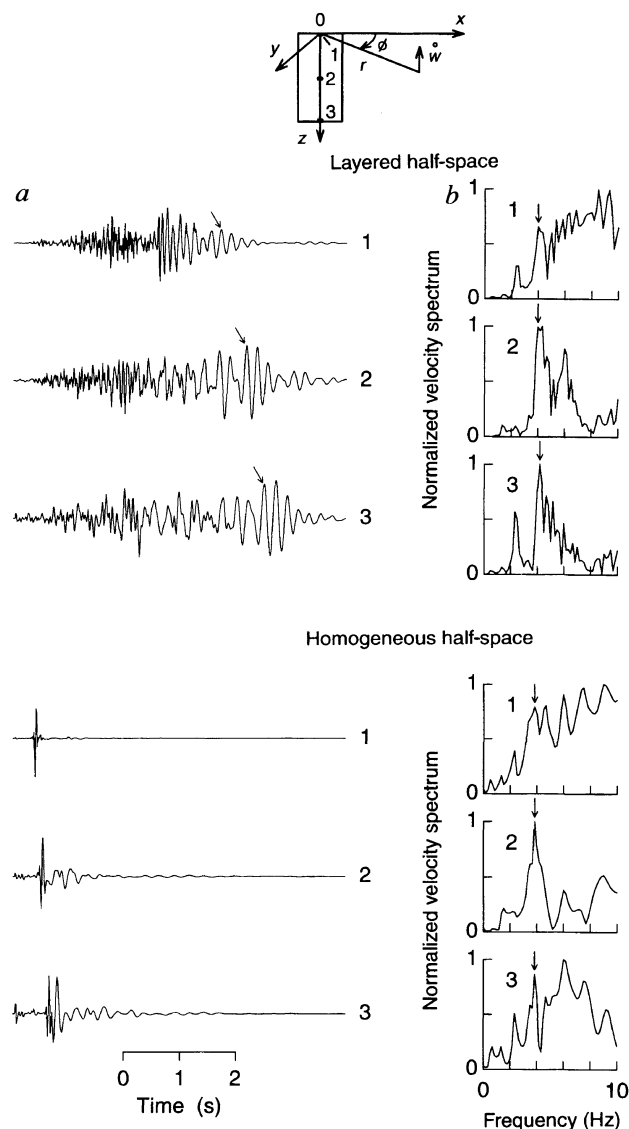

FIG. 4 Comparisons between ground velocity responses due to the excitation of a fluid-filled crack embedded in a layered half-space and those obtained for the same source buried in a homogeneous half-space. The layered half-space has three layers, with the following P- and S-wave velocities (km s^{-1}), densities (g cm^{-3}) and thicknesses (m): layer 1 (0.65, 0.35, 2.65, 30); layer 2 (1.25, 0.72, 2.70, 75); layer 3 (2.50, 1.44, 2.75, ∞). The homogeneous half-space has parameters identical to those of layer 3 in that structure. The crack geometry is shown in the cartesian coordinates at the top of the figure. All the synthetics are for a 100-m-wide vertical crack extending from the free surface to a depth of 200 m. The crack is excited by a step in pressure applied over a small area of the crack just below the free surface, at 100 m depth, or at 200 m depth. Each synthetic represents a vertical component $\dot{w}$ calculated at a distance r of 1 km and azimuth ϕ of 25 degrees. The numbers (1, 2, 3) attached to the seismograms and spectra refer to the locations of the pressure transient shown in the sketch. a, Synthetic seismograms. The slanted arrows point to the short-duration quasi-monochromatic coda associated with crack resonance in the synthetics calculated for the layered structure. b, Spectra of the seismograms shown at the left. The arrows mark one of the resonant peaks due to the source; this spectral peak is present in all models.

the LP signature from VT events rather hopeless. Fortunately, the spectral character of the signal is helpful here.

The spectra derived from the synthetics (Fig. 4b) show that the source has distinct peaks which can be identified among spectral peaks due to path effects. For example, source effects are clearly identified in the homogeneous half-space where all spectra show a peak near 3.8 Hz due to crack resonance (see arrows above individual spectra). Other peaks due to the source are also present, although less obvious because of the dependence of their excitation on the position of the pressure transient triggering the crack resonance. The dominant peak near 3.8 Hz is also present in the spectra obtained for the layered structure, the effect of which is to introduce additional peaks due to near-surface resonances. The peaks associated with path effects, however, are strongly dependent on the source–receiver configuration, whereas those due to the source are not. This is demonstrated in Fig. 5a for a crack buried at various depths in the Pu'u O'o structure.

The synthetics shown in Fig. 5a incorporate the same source–receiver geometry and model parameters but assume the position of the pressure transient to be fixed at the centre of the crack. Three source depths ($h = 0$, 105 and 300 m) are used to assess the relative importance of path effects for sources that reach up to the surface, reach up to the bottom of layer 2, or are completely decoupled from those shallow layers. Both homogeneous and layered media produce roughly the same spectra, which all display a peak at a frequency near 3.8 Hz due to the source. The effect of structure on the spectra of the deeper sources in or at the top of the half-space (layer 3 in the layered model) is insignificant (see bottom two panels for $h = 105$ and 300 m in Fig. 5a), and although path effects are stronger for the surficial source (see top panel in Fig. 5a), the dominant source peak is still easily identifiable. These calculations demonstrate that, to first order, source resonances are stable features in the radiated spectra, and suggest that these resonances may be separated from resonances due to path effects even for low-impedance sources. In practical situations, the identification of source effects can be enhanced through the expedient of stacking data from distinct receivers.

The above model may be used to illustrate the relationship between LP events and sustained tremor. Two examples in Fig. 5b compare models of tremor generation in the Pu'u O'o structure. The model geometry is identical to that used in Fig. 5a. I assumed that a complex pressure–time history could cause sequential excitation of the crack and modelled this source excitation by superposing identical waveforms with random time delays. The original waveforms generated by the step excitation of the crack and the waveforms obtained by superposition of delayed versions of those synthetics are shown at the top of the figure for two crack depths. An identical sequence of random time delays between 0 and 1 s generated from five-digit random numbers[58] was used to produce the latter results. The spectra of the resulting synthetics (see bottom two panels in Fig. 5b) share common peaks although they differ markedly in their detailed structure. The spectra shown in the bottom panel, in particular, suggest that source excitation complexity can significantly affect the radiated spectrum by splitting and modulating the amplitudes of the resonant peaks associated with the step response and by contributing additional peaks to that spectrum. Of particular interest is the strong dependence of the band of radiated energy on source depth, due in large part to the amplification and splitting of spectral peaks below 4 Hz in the deeper source (bottom panel) produced by random excitations. These waveforms and spectra agree qualitatively with those observed for tremor at Pu'u O'o[59] and indicate that path effects and effects that are characteristic of the fluid dynamics may both contribute to the observed spectral complexity for shallow sources. Obviously, the complexities of the driving mechanisms of tremor make this a much more difficult source to study than the LP event, and it is only under the more favourable circumstances of a tremor source with stationary spatio-temporal characteristics that quantification of the source mechanisms may be feasible.

Under such circumstances the technique of spectral stacking may again be helpful in extracting stationary peaks due to sustained source resonance.

Quantitative analysis at Redoubt volcano

The reawakening of Redoubt volcano on 13 December, 1989, after 23 years of quiescence, was heralded by the gradual onset of repetitive LP events. This activity soon evolved into an intense swarm that lasted 23 hours and terminated with the initial major eruption on 14 December, which blew ash to an altitude in excess of 10,000 m (refs 2,60). Several outstanding features of the swarm were immediately recognized[2], as follows: a rapidly accelerating rate of seismic energy release over the first 18 hours of activity, followed by a decline coinciding with the emergence of sustained tremor in the final 5 hours before the eruption; nearly identical signatures for individual events in the swarm; dilatational first motions on all stations of the network for all LP events with clear P phases; and a magnitude range from −0.4 to 1.6 for the entire sequence. Detailed spectral analyses performed subsequently revealed that both LP events and tremor had similar spectra
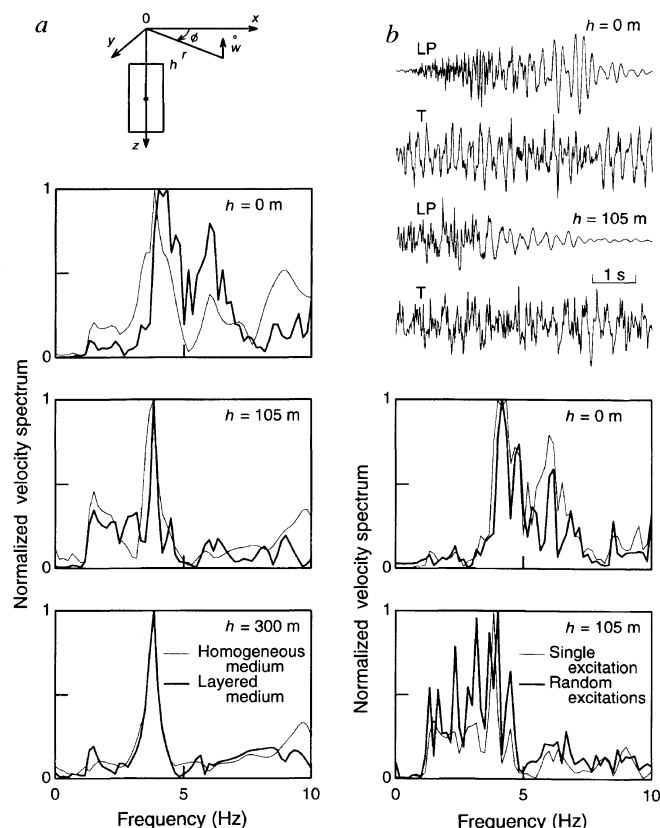

FIG. 5 Dependence of synthetics on crack depth and crack excitation. The crack geometry is shown in the cartesian coordinates at the upper left. All synthetics are for a 100-m-wide, 200-m-long, vertical crack excited by a pressure transient applied at the centre of the crack. Each synthetic represents a vertical component of ground velocity w calculated at a distance r of 1 km and azimuth ϕ of 25°. a, Comparisons between spectra obtained for a crack embedded in a homogeneous half-space and those derived for the same crack embedded in a layered half-space. The spectra are calculated for a step excitation of a crack buried at depths $h = 0$ m (top), $h = 105$ m (middle), and $h = 300$ m (bottom). The spectra shown for $h = 0$ m are the same as those depicted for case 2 in Fig. 4b. b, Comparisons between ground velocities and spectra calculated for a single step excitation and those derived for multiple step excitations of a crack embedded in a layered structure. Top, synthetics obtained for a single excitation (LP) and synthetics obtained by delaying and superposing multiple copies of the LP waveforms (T) for two crack depths $h = 0$ m and $h = 105$ m. Bottom, spectra of the seismograms shown above.

marked by several dominant and subdominant peaks common to stations covering a wide range of azimuths and distances from the source[2], while careful location and error analyses established that this activity originated from a single point source 1.4 km below the crater floor[36].

These features were found to be compatible with those produced by the resonant excitation of a fluid-driven crack and yielded the following parameters for the LP source[2]: crack length, 280–380 m; crack width, 140–190 m; crack aperture, 0.05–0.20 m; crack stiffness, 100–200; sound speed of fluid, 0.8–1.3 km s^{-1}; compressional wavespeed of rock, 5.1 km s^{-1}; density ratio of fluid to rock, about 0.4; and ratio of bulk modulus of fluid to rigidity of rock, 0.03–0.07. Crack excitation was fitted by an impulsive pressure drop in the range 0.4–40 bar. These parameters, along with the spatio-temporal characteristics of the pressure transient and observed intermittency, collectively were found to be consistent with forced crack excitations associated with unsteady choked flow conditions[2].

A conceptual model of the processes that may have characterized the pre-eruptive sequence observed at Redoubt is shown in Fig. 6a. The sketch shows the old dome capping the vent, the hydrothermal system, shallow magma chamber, and LP source located between these two reservoirs. The evidence for a shallow magma chamber comes from a tomographic study conducted at Redoubt in 1991, in which a volume of approximately 2–3 km^3 with P- to S-wave velocity ratio 4% higher than average was found centred 2.5 km beneath the crater and 1–2 km north of the eruptive vent[61]. This small volume is located immediately beneath and to the north of the source of the LP swarm. Petrological data provide evidence for a magma-mixing event preceding the start of the eruption[62], which is thought to have been the source of the excess pressure driving the sequence[63]. Accordingly, the initiation of the swarm may be interpreted as representing the failure of a pressure-relief valve connecting a deeper supercharged magma-dominated reservoir to a shallow low-pressure hydrothermal system. The sustained rate of 3–5 LP events per minute observed during the first 18 hours of the swarm[2] may then be viewed as the result of unsteady choking of a supersonic flow of magmatic steam driven by the pressure gradient existing between the two reservoirs. By the same token, the emergence of sustained tremor 5 hours before the eruption may represent a change in choked-flow regime associated with a gradual weakening of the pressure gradient driving the flow[64].

The graph in Fig. 6b gives a schematic representation of the pressure histories in the magma chamber and hydrothermal system, and pressure gradient between these two reservoirs, along with significant events inferred to have occurred during the 23-hour-long pre-eruptive phase. Injection of a more mafic magma into the base of the magma reservoir[62] represents the initial event that triggered magmatic convection and increased exsolution of volatiles leading to rapid pressurization of the system. At some time during this pressurization phase, critical pressure was reached and either a fracture was created or a pre-existing fissure was dilated and communication was opened to the overlying lower-pressure hydrothermal system. The pressure gradient between the two systems then drove magmatic steam through this conduit, and LP activity was triggered by unsteady choked flow in response to fluctuations of outlet pressure associated with the reaction of the upper reservoir to the injection of mass and heat from below[65]. Initially, the hydrothermal system may have responded to the increased heat injection into its base by accelerated convection that would have manifested itself in increased steam emissions at the summit of Redoubt, and indeed observations of the volcano a few days before the eruption seem to indicate that such may have been the case. Later in the swarm sequence, the import of heat started to exceed the capacity of the hydrothermal system to evacuate so that heat and pressure started to rise in that system as well. Eventually, the pressure gradient driving the LP source started to decrease and the flow regime inside the crack changed from intermittent, high-

FIG. 6 Conceptual model of pre-eruptive processes at Redoubt volcano on 13–14 December 1989. a, Sketch illustrating the spatial relationship between the stationary LP source, the magma chamber inferred from tomography, the hydrothermal system, and lava dome emplaced during the previous eruption in 1966. b, Cartoon sketching the pressurization of the magma chamber, P_m, and associated pressurization of the hydrothermal system, P_h, along with the pressure difference between these two systems, ΔP. Significant events in the pressurization history are indicated by arrows. Note that the pressure histories depicted are heavily smoothed to enhance gross behaviour (in reality, these curves are expected to display small-scale fluctuations superimposed on the smoothed trends depicted). Episodes of LP activity, hydrothermal convection and magmatic convection are shown in boxes beneath the graph, where the horizontal extent of the boxes represents the observed duration of LP activity and inferred durations of hydrothermal and magmatic convections.
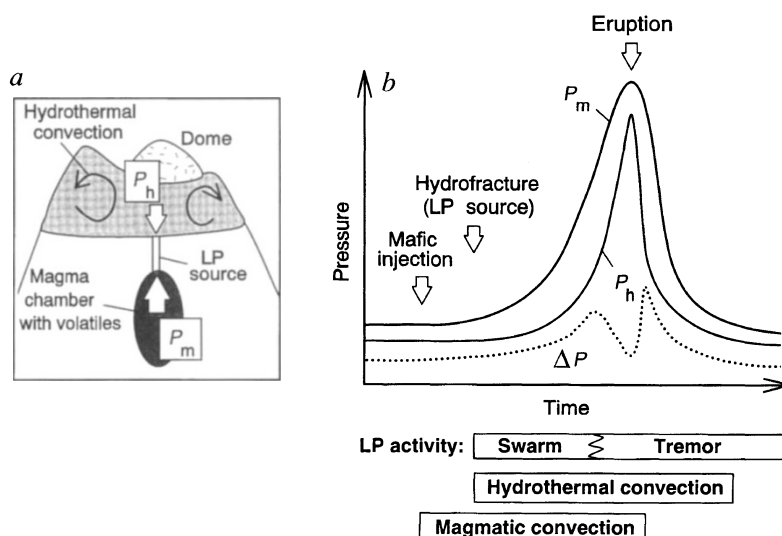
amplitude pressure transients producing discrete LP events, to sustained, low-amplitude pressure fluctuations producing tremor. The pressure gradient between the two reservoirs continued to decrease for a few hours as the pressure kept on rising in both of them, finally culminating in the dome-destroying eruption.

Future directions

The above considerations point to the importance of shallow LP activity in forecasting the onset and climactic stages of an important class of highly hazardous volcanic eruptions—namely, the stratovolcanoes bordering the highly populated western margin of the Americas, as well as those of the Mexican–Caribbean, Mediterranean and Pacific Basin regions of the world. To benefit fully from this new understanding of the processes underlying volcano behaviour, however, further elaboration of the physical model of LP activity will be required. Foremost among the challenges facing volcano seismologists is a better understanding of the excitation mechanisms of LP events and tremor in relation to the overall process of fluid percolation in a volcano[43]. The challenge is best exemplified in the activity of deep LP events (> 10 km depth).

Although a direct link has been observed between shallow LP activity and eruptions, the relationship with deeper LP events is less clear. Long-period events occurred at depths near 30 km at Pinatubo in early June 1991, where they were attributed to a basaltic intrusion which is thought to have triggered the processes leading to the cataclysmic 15 June eruption[50,66]. On the other hand, LP events are regularly observed at depths of 30–60 km beneath Kilauea, where their occurrence appears to be more directly related to deep magma supply dynamics than surface activity[43]. A low background of deep LP events is not uncommon, and may indeed be the rule rather than the exception as accumulating observations now increasingly suggest[67-70]. The difficulty here has to do with our lack of knowledge concerning the character and dynamics of deep-seated fluid transport under volcanoes. Another difficulty stems from the wide range of timescales involved in volcanic processes. Short-period seismology, which typically covers the bandwidth 1–20 Hz, is not by itself sufficient to resolve longer-term processes such as those associated with mass transport. For example, the timescale of mass transport between the magma and hydrothermal reservoirs during the precursory sequence leading to the 1989 eruption of Redoubt volcano is about a day, which is well beyond the response capability of short-period instruments. To document fully the relationship between point-like LP activity and the overall pathway structure used by eruptive fluids, broadband instruments are required. Sacks–Evertson borehole strain-meters have proven to be quite useful in volcanic applications[71], and arrays of such instruments coupled with three-component broadband seismo-

graphs may present unprecedented opportunities to monitor the movements of magmatic and hydrothermal fluids before eruptions. Progress in broadband volcano seismology has already been made in that direction with encouraging results[72-74].

A fuller understanding of the excitation mechanisms of LP events and tremor may be achieved through further modelling efforts. Kinematic models such as those discussed above (in which conduit resonance is excited via an arbitrary initial condition; see Figs 3–5) will need to be replaced by dynamic models (in which the conduit is self-excited by some disturbance in the flow process) if we are to understand better the link between seismic signals and fluid processes in a volcano. New studies have brought to light self-excitation mechanisms inherent to fluid nonlinearity that point the way in that direction[65,75]. With the advent of more powerful computers, numerical studies of multi-phase flows are improving our knowledge of both the micro- and macrophysics of such flows. Computer models can now be developed to study various types of flow instabilities[76], and laboratory experiments can be used to anchor numerical results and give further insights into self-excited pressure oscillations[64,75] that may be adequate models for LP and tremor sources. □

B. A. Chouet is at the US Geological Survey, 345 Middlefield Road, MS 977, Menlo Park, California 94025, USA.

1. Shaw, H. R. J. geophys. Res. 90, 11275–11288 (1985).
2. Chouet, B. A., Page, R. A., Stephens, C. D., Lahr, J. C. & Power, J. A. J. Volcan. geotherm. Res. 62, 95–135 (1994).
3. Koyanagi, R. Y., Chouet, B. & Aki, K. Prof. Pap. U.S. geol. Surv. 1350, 1221–1257 (1987).
4. Endo, E. T., Malone, S. D., Noson, L. L. & Weaver, C. S. Prof. Pap. U.S. geol. Surv. 1250, 93–107 (1981).
5. Pinatubo Volcano Observatory Team Eos 72, 545–555 (1991).
6. Power, J. A., Jolly, A. D., Page, R. A. & McNutt, S. R. Bull. U.S. geol. Surv. 2139, 149–159 (1995).
7. Tilling, R. I. & Dvorak, J. J. Nature 363, 125–133 (1993).
8. Lockwood, J. P. et al. Eos 66, 169–171 (1985).
9. Ida, Y. Nature 352, 571–572 (1991).
10. Venzke, E., Wunderman, R. & Peng, G. (eds) Smithsonian Instn Bull. Global Volc. Net. 19, 4–7 (1994).
11. Newhall, C. G. & Dzurisin, D. Bull. U.S. geol. Surv. 1855, 7–16 (1988).
12. McNutt, S. R. Encyclopedia of Earth Science Vol. 4, 417–425 (Academic, 1992).
13. Barberi, F., Bertagnini, A., Landi, P. & Principe, C. J. Volcan. geotherm. Res. 52, 231–246 (1992).
14. Minakami, T. in Physical Volcanology (eds Civetta, L., Gasparini, P., Luongo, G. & Rapolla, A.) 1–27 (Elsevier, New York, 1974).
15. Kagiyama, T., Gyoda, N., Koyama, E. & Tsuji, H. in Comparative Studies of Physical Background of Volcanic Activity and its Relation to Eruption Disasters (ed. Okada, H.) 92–101 (Hokkaido Univ., Hokkaido, 1985).
16. Shimozuru, D. & Kagiyama, T. in Volcanic Hazards (ed. Latter, J. H.) 504–512 (Springer, Berlin, 1989).
17. Rep. Coordin. Committee on Prediction of Volcanic Eruptions Vol 41, 64–77 (1988).
18. Ukawa, M. J. Volcan. geotherm. Res. 55, 33–50 (1993).
19. Havskov, J., De la Cruz-Reyna, S., Singh, S. K., Medina, F. & Gutiérrez, C. Geophys. Res. Lett. 10, 293–296 (1983).
20. Stephens, C. D., Chouet, B. A., Page, R. A., Lahr, J. C. & Power, J. A. J. Volcan. geotherm. Res. 62, 153–182 (1993).
21. Muñoz, F. A. et al. Eos 74, 281–287 (1993).

22. Okada, H., Nishimura, Y., Miyamachi, H., Mori, H. & Ishihara, K. *Bull. volcan. Soc. Jap.* **35,** 175–203 (1990).
23. Gil Cruz, F., Meyer, H. J., Chouet, B. & Harlow, D. *Hawaii Symp. on How Volcanoes Work, Diamond Jubilee (1912–1987)* 90 (Hawaiian Volcano Observatory, Hilo, Hawaii, 1987).
24. Martinelli, B. *J. Volcan. geotherm. Res.* **41,** 297–314 (1990).
25. Venzke, E., Wunderman, R. & Peng, G. (eds) *Smithsonian Instn Bull. Global Volc. Net.* **17(6),** 11 (1992).
26. Malone, S. D., Endo, E. T., Weaver, C. S. & Ramey, J. W. *Prof. Pap. U.S. geol. Surv.* **1250,** 803–813 (1981).
27. Qamar, A., St Lawrence, W., Moore, J. N. & Kendrick, G. *Bull. seism. Soc. Am.* **73,** 1797–1813 (1983).
28. Swanson, D. A. et al. *J. Geodynamic.* **3,** 397–423 (1985).
29. Weaver, C. S., Grant, W. C., Malone, S. D. & Endo, E. T. *Prof. Pap. U.S. geol. Surv.* **1250,** 109–121 (1981).
30. Fehler, M. & Chouet, B. *Geophys. Res. Lett.* **9,** 1017–1020 (1982).
31. Fischer, T. P. et al. *Nature* **368,** 135–137 (1994).
32. Nishi, K. A. *Disaster Prev. Res. Inst. Kyoto Univ.* **27 B-1,** 29–34 (1984).
33. Venzke, E., Wunderman, R. & Peng, G. (eds) *Smithsonian Instn Bull. Global Volc. Net.* **17(12),** 2–4 (1992).
34. Venzke, E., Wunderman, R. & Peng, G. (eds) *Smithsonian Instn Bull. Global Volc. Net.* **18(6),** 2–3 (1993).
35. Minakami, T. *Bull. Earthquake Res. Inst. Univ. Tokyo* **38,** 497–544 (1960).
36. Lahr, J. C., Chouet, B. A., Stephens, C. D., Power, J. A. & Page, R. A. *J. Volcan. geotherm. Res.* **62,** 137–151 (1994).
37. Eaton, J. P., Richter, D. H. & Krivoy, H. L. *Prof. Pap. U.S. geol. Surv.* **1350,** 1307–1336 (1987).
38. Chouet, B. in *Volcanic Seismology* (eds Gasparini, P., Scarpa, R. & Aki, K.) 133–156 (Springer, Berlin, 1992).
39. Shaw, H. R. in *Physics of Magmatic Processes* (ed. Hargraves, R. B.) 201–264 (Princeton Univ. Press, 1980).
40. Takeo, M. *Phys. Earth planet. Inter.* **32,** 241–264 (1983).
41. Peck, D. L. & Minakami, T. *Geol. Soc. Am. Bull.* **79,** 1151–1166 (1968).
42. Chouet, B. *J. geophys. Res.* **84,** 2315–2330 (1979).
43. Shaw, H. R. & Chouet, B. *J. geophys. Res.* **96,** 10191–10207 (1991).
44. Hill, D. P. *J. geophys. Res.* **82,** 1347–1352 (1977).
45. Aki, K. & Koyanagi, R. *J. geophys. Res.* **86,** 7095–7109 (1981).
46. Kamo, K., Furuzawa, T. & Akamatsu, J. *Bull. Volcan. Soc. Japan.* **22,** 41–58 (1977).
47. Wolfe, E. W. *Earthquakes & Volcanoes* **23(1)** 5–37 (1992).
48. Ukawa, M. *J. Volcan. geotherm. Res.* **55,** 33–50 (1993).
49. Miller, T. P. *J. Volcan. geotherm. Res.* **62,** 197–212 (1994).

50. White, R. A., Harlow, D. H. & Chouet, B. A. *Eos* (suppl.) **73(43),** 347 (1992).
51. Chouet, B. *J. geophys. Res.* **90,** 1881–1893 (1985).
52. Crosson, R. S. & Bame, D. A. *J. geophys. Res.* **90,** 10237–10247 (1985).
53. Chouet, B. *J. geophys. Res.* **91,** 13967–13992 (1986).
54. Chouet, B. *J. geophys. Res.* **93,** 4373–4400 (1988).
55. Aki, K., Fehler, M. & Das, S. *J. Volcan. geotherm. Res.* **2,** 259–287 (1977).
56. Kieffer, S. W. *J. geophys. Res.* **82,** 2895–2904 (1977).
57. Ferrazzini, V., Aki, K. & Chouet, B. *J. geophys. Res.* **96,** 6199–6209 (1991).
58. Abramowitz, M. & Segun, I. A. *Handbook of Mathematical functions* 991 (Dover, New York, 1972).
59. Goldstein, P. & Chouet, B. *J. geophys. Res.* **99,** 2637–2652 (1994).
60. Brantley, S. R. *U.S. geol. Surv. Circ.* **1061,** 1–33 (1990).
61. Benz, H. M. et al. *J. Geophys. Res.* (in the press).
62. Swanson, S. E., Nye, C. J., Miller, T. P. & Avery, V. F. *J. Volcan. geotherm. Res.* **62,** 453–468 (1994).
63. Sparks, S. R. J., Sigurdsson, H. & Wilson, L. *Nature* **267,** 315–318 (1977).
64. Meier, G. E. A., Grabitz, G., Jungowsky, W. M., Witczak, K. J. & Anderson, J. S. *Mitteilungen aus dem Maz-Plank Institut für Strömungsforschung und der Aerodynamischen Versuchsanstalt* **65,** 1–172 (1978).
65. Morrissey, M. M. & Chouet, B. A. (abstr.) *IUGG XXI General Assembly* A461 (IUGG, Boulder, 1995).
66. Pallister, J. S., Hoblitt, R. P. & Reyes, A. G. *Nature* **356,** 426–428 (1992).
67. Pitt, A. M. & Hill, D. P. *Geophys. Res. Lett.* **21,** 1679–1682 (1994).
68. Ukawa, M. *Nat. Res. Center for Disaster Prev.* **37,** 129–133 (1984).
69. Ukawa, M. & Ohtake, M. *J. geophys. Res.* **92,** 12649–12663 (1987).
70. Hasegawa, A., Zhao, D., Hori, S., Yamamoto, A. & Horiuchi, S. *Nature* **352,** 683–689 (1991).
71. Linde, A. T., Agustsson, K., Sacks, I. S. & Stefansson, R. *Nature* **365,** 737–740 (1993).
72. Kanamori, H., Given, J. W. & Lay, T. *J. geophys. Res.* **89,** 1856–1866 (1984).
73. Uhira, K. & Takeo, M. *J. geophys. Res.* **99,** 17775–17789 (1994).
74. Kawakatsu, H., Ohminato, T. & Ito, H. *Geophys. Res. Lett.* **21,** 1963–1966 (1994).
75. Julian, B. R. *J. geophys. Res.* **99,** 11859–11877 (1994).
76. Harlow, F. H. & Amsden, A. A. *J. comput. Phys.* **17,** 19–52 (1975).
77. Meier, G. E. A., Szumowski, A. P. & Selerowicz, W. C. *Prog. Aerospace Sci.* **27,** 145–200 (1990).

Structural similarity between TAFs and the heterotetrameric core of the histone octamer

Xiaoling Xie*†, **Tetsuro Kokubo**‡#, **Steven L. Cohen**§, **Urooj A. Mirza**§, **Alexander Hoffmann**‖#, **Brian T. Chait**§, **Robert G. Roeder**‖, **Yoshihiro Nakatani**‡ & **Stephen K. Burley***†¶

Laboratories of * Molecular Biophysics, § Mass Spectrometry and Gaseous Ion Chemistry, and ‖ Biochemistry and Molecular Biology, and † Howard Hughes Medical Institute, The Rockefeller University, 1230 York Avenue, New York, New York 10021, USA
‡ National Institutes of Child Health and Human Development, National Institutes of Health, Bethesda, Maryland 20892, USA

A complex of two TFIID TATA box-binding protein-associated factors (TAF$_{II}$s) is described at 2.0 Å resolution. The amino-terminal portions of dTAF$_{II}$42 and dTAF$_{II}$62 from *Drosophila* adopt the canonical histone fold, consisting of two short α-helices flanking a long central α-helix. Like histones H3 and H4, dTAF$_{II}$42 and dTAF$_{II}$62 form an intimate heterodimer by extensive hydrophobic contacts between the paired molecules. In solution and in the crystalline state, the dTAF$_{II}$42/dTAF$_{II}$62 complex exists as a heterotetramer, resembling the (H3/H4)$_2$ heterotetrameric core of the histone octamer, suggesting that TFIID contains a histone octamer-like substructure.

EUKARYOTIC transcription initiation and its regulation are best understood for genes transcribed by RNA polymerase II (Pol II) with the general transcription factors TFIIA, TFIIB, TFIID, TFIIE, TFIIF, TFIIG/J, TFIIH and TFIII (reviewed in refs 1,2). In some cases, this process begins with recognition of the TATA element within the core promoter by the DNA-binding subunit of

TFIID (TATA box-binding protein, TBP), forming a multi-protein–DNA complex that coordinates accretion of class II initiation factors and Pol II into a preinitiation complex (PIC) (reviewed in ref. 3). TFIIB is the next general factor to enter the PIC, creating a TFIIB–TFIID–DNA platform that is recognized by Pol II plus TFIIF. *In vivo*, Pol II transcription depends on TFIIE and TFIIH, and possibly TFIIA. Once PIC assembly is complete, and nucleoside triphosphates are present, strand separation occurs to give an open complex, the large subunit of Pol II is phosphorylated, and Pol II initiates transcription and is

¶ To whom correspondence should be addressed.
# Present address: Division of Gene Function in Animals, Nara Institute of Science and Technology, 8916-5 Takayama, Ikoma, Nara 630-01, Japan (T.K.); Department of Biology, Massachusetts Institute of Technology, Cambridge, Massachusetts 02139, USA (A.H.).